



# Optimized antiangiogenic reprogramming of the tumor microenvironment potentiates CD40 immunotherapy

Abhishek S. Kashyap<sup>a,1,2</sup>, Martina Schmittnaegel<sup>b,1,3</sup>, Nicolò Rigamonti<sup>b,4</sup>, Daniela Pais-Ferreira<sup>b</sup>, Philipp Mueller<sup>a,5</sup>, Melanie Buchi<sup>a</sup>, Chia-Huey Ooi<sup>c</sup>, Matthias Kreuzaler<sup>a</sup>, Petra Hirschmann<sup>d</sup>, Alan Guichard<sup>b</sup>, Natascha Rieder<sup>e</sup>, Ruben Bill<sup>a,6</sup>, Frank Herting<sup>e</sup>, Yvonne Kienast<sup>e</sup>, Stefan Dirnhofer<sup>d</sup>, Christian Klein<sup>f</sup>, Sabine Hoves<sup>e</sup>, Carola H. Ries<sup>e</sup>, Emily Corse<sup>f</sup>, Michele De Palma<sup>b,1,2</sup>, and Alfred Zippelius<sup>a,g,1,2</sup>

<sup>a</sup>Department of Biomedicine, University Hospital Basel and University of Basel, 4031 Basel, Switzerland; <sup>b</sup>Swiss Institute for Experimental Cancer Research (ISREC), School of Life Sciences, École Polytechnique Fédérale de Lausanne (EPFL), 1015 Lausanne, Switzerland; <sup>c</sup>Pharma Research and Early Development, Pharmaceutical Sciences, Roche Innovation Center Basel, 4070 Basel, Switzerland; <sup>d</sup>Institute of Medical Genetics and Pathology, University Hospital Basel, 4031 Basel, Switzerland; <sup>e</sup>Pharma Research and Early Development, Roche Innovation Center Munich, 82377 Penzberg, Germany; <sup>f</sup>Pharma Research and Early Development, Roche Innovation Center Zurich, 8952 Schlieren, Switzerland; and <sup>g</sup>Medical Oncology, University Hospital Basel, 4031 Basel, Switzerland

Edited by Napoleone Ferrara, University of California San Diego, La Jolla, CA, and approved November 15, 2019 (received for review February 6, 2019)

Cancer immunotherapies are increasingly combined with targeted therapies to improve therapeutic outcomes. We show that combination of agonistic anti-CD40 with antiangiogenic antibodies targeting 2 proangiogenic factors, vascular endothelial growth factor A (VEGFA) and angiopoietin 2 (Ang2/ANGPT2), induces pleiotropic immune mechanisms that facilitate tumor rejection in several tumor models. On the one hand, VEGFA/Ang2 blockade induced regression of the tumor microvasculature while decreasing the proportion of nonperfused vessels and reducing leakiness of the remaining vessels. On the other hand, both anti-VEGFA/Ang2 and anti-CD40 independently promoted proinflammatory macrophage skewing and increased dendritic cell activation in the tumor microenvironment, which were further amplified upon combination of the 2 treatments. Finally, combined therapy provoked brisk infiltration and intratumoral redistribution of cytotoxic CD8<sup>+</sup> T cells in the tumors, which was mainly driven by Ang2 blockade. Overall, these nonredundant synergistic mechanisms endowed T cells with improved effector functions that were conducive to more efficient tumor control, underscoring the therapeutic potential of antiangiogenic immunotherapy in cancer.

angiogenesis | immunotherapy | CD40 | VEGFA | angiopoietin

Reinvigoration of T cell function by PD-1 and/or CTLA-4 immune checkpoint blockade can result in striking clinical responses in selected cancer types, yet these treatments are effective only in a minority of cancer patients (1, 2). Agonistic targeting of CD40 represents an alternative approach for promoting antitumor immunity (3). CD40, a tumor necrosis factor (TNF)-receptor superfamily member, is primarily expressed on antigen-presenting cells (APCs), including dendritic cells (DCs), B cells, macrophages, and monocytes, as well as nonhematopoietic cells and subsets of cancer cells. Ligation of CD40 with CD40L (CD154) results in direct activation of APCs, which involves up-regulation of costimulatory and MHC molecules and production of proinflammatory cytokines. This is a key step in the generation of an antitumor immune response, and there is evidence that agonistic CD40 antibodies facilitate rejection of established tumors in different mouse models of cancer (4, 5). CD40-targeting antibodies with varying binding affinity are evaluated in clinical trials, including selicrelumab (RG7876), dacetuzumab, APX 005M, ChiLob 7/4, and lucatumumab (3, 6). While toxicity appears manageable and durable anticancer responses were observed, clinical activity of single-agent CD40 antibodies appears to be rather modest, with response rates of <20% in patients (6). Clinical efforts are currently directed at exploring combinations of anti-CD40 with chemotherapy, PD-1/PD-L1 blocking antibodies (e.g., NCT02304393, NCT03502330, NCT03123783, and NCT02706353), or antiangiogenic antibodies bevacizumab (Avastin; a clinically approved antivasculature endothelial growth factor A [anti-VEGFA] antibody) and vanucizumab (an anti-VEGFA/Ang2 bispecific antibody) (NCT02665416).

Angiogenesis contributes to tumor growth and progression by inducing and maintaining an acidic/hypoxic and immunosuppressive environment (7, 8). The tumor frequently harbors dysfunctional blood vessels, which limit T cell trafficking (7). Furthermore, several proangiogenic growth factors, primarily VEGFA, limit DC

## Significance

Cancer immunotherapy demonstrates clinical efficacy in selected cancer types. Yet, as the majority of patients do not respond to the most effective immunotherapeutics, novel immunotherapy combinations are extensively investigated. There is increasing clinical interest in combining cancer immunotherapies with antiangiogenic agents, particularly VEGFA pathway inhibitors. Here we show that anti-CD40 immunotherapy increases CD8<sup>+</sup> T cell infiltration in the tumor, yet tumor regression is achieved more robustly when anti-CD40 is combined with dual Ang2 and VEGFA blockade, but not VEGFA inhibition alone. Tumor regression was associated with proinflammatory skewing of the tumor microenvironment and intratumoral redistribution of CD8<sup>+</sup> T cells. These data emphasize the rationale for blocking Ang2 as a vascular-modulatory strategy in combination with T cell-targeting immunotherapies.

Author contributions: A.S.K., M.S., P.M., F.H., Y.K., C.K., C.H.R., E.C., M.D.P., and A.Z. designed research; A.S.K., M.S., N. Rigamonti, D.P.-F., P.M., M.B., M.K., P.H., A.G., N. Rieder, R.B., F.H., and S.D. performed research; R.B., S.H., and C.H.R. contributed new reagents/analytic tools; A.S.K., M.S., N. Rigamonti, D.P.-F., P.M., C.-H.O., A.G., R.B., F.H., Y.K., S.D., C.K., S.H., and E.C. analyzed data; and A.S.K., M.S., A.G., E.C., M.D.P., and A.Z. wrote the paper.

Competing interest statement: M.S., C.-H.O., N. Rieder, F.H., Y.K., C.K., S.H., C.H.R., and E.C. are former or current Roche employees. C.-H.O., N. Rieder, F.H., C.K., S.H., and C.H.R. are Roche stock holders. M.D.P. and A.Z. received research funding from Roche. The other authors declare that they have no competing interests.

This article is a PNAS Direct Submission.

This open access article is distributed under [Creative Commons Attribution-NonCommercial-NoDerivatives License 4.0 \(CC BY-NC-ND\)](https://creativecommons.org/licenses/by-nc-nd/4.0/).

Data deposition: Primary RNA-seq datasets have been deposited in the Gene Expression Omnibus (GEO), <https://www.ncbi.nlm.nih.gov/geo/> under accession code GSE94920.

<sup>1</sup>A.S.K., M.S., M.D.P., and A.Z. contributed equally to this work.

<sup>2</sup>To whom correspondence may be addressed. Email: abhishek.kashyap@unibas.ch, michele.depalma@epfl.ch, or alfred.zippelius@usb.ch.

<sup>3</sup>Present address: Pharma Research and Early Development, Roche Innovation Center Munich, 82377 Penzberg, Germany.

<sup>4</sup>Present address: Molecular Partners, 8952 Schlieren, Switzerland.

<sup>5</sup>Present address: Boehringer Ingelheim Pharma GmbH & Co, 88397 Biberach an der Riss, Germany.

<sup>6</sup>Present address: Centre for Systems Biology, Massachusetts General Hospital, Boston, MA 02114.

This article contains supporting information online at <https://www.pnas.org/lookup/suppl/doi:10.1073/pnas.1902145116/-DCSupplemental>.

First published December 30, 2019.

maturation and promote the accumulation of immunosuppressive immature myeloid cells in tumors (9–11). Blocking proangiogenic growth factors may, therefore, not only inhibit angiogenesis but also relieve immunosuppression in tumors. Several antiangiogenic therapies that block VEGFA signaling are tested both preclinically and clinically. Yet, anti-VEGFA therapies combined with standard-of-care treatments increase progression-free survival by only 3 to 6 mo with minor, if any, improvement of overall survival rates, depending on the cancer type (12). In glioblastoma patients and various mouse cancer models, resistance to anti-VEGFA therapy may be associated with the induction of the proangiogenic factor angiopoietin 2 (Ang2/ANGPT2), a ligand of the TIE2/TEK receptor (13–15). In various tumor models, Ang2/Tie2 inhibition reduces tumor growth in the presence of active VEGFR signaling; nevertheless, greater inhibitory effects on angiogenesis and tumor growth are observed with combined blockade of Ang2 and VEGFA (15–22). Additionally, Ang2 blockade induces blood vessel normalization, blocks metastasis, and promotes a proinflammatory tumor microenvironment (9, 17, 20, 23–25). Ang2 inhibition, with or without concurrent VEGFA inhibition, is being evaluated in clinical trials in combination with chemotherapy and other anticancer agents (14, 26).

Preclinically, both DC101, an anti-VEGFR2 antibody, and A2V, an anti-VEGFA/Ang2 bispecific antibody, have been shown to increase the efficacy of anti-PD-1/PD-L1 immunotherapy by increasing T cell trafficking in tumors (22, 27). Several clinical studies (NCT03439891, NCT03277924, NCT03616691, and NCT03074513) are evaluating the efficacy of antiangiogenic therapy in combination with immune checkpoint blockade (1, 2, 26, 28, 29). Anti-CD40 immunotherapy (3–6, 30, 31) might represent a complementary approach to immune checkpoint inhibitors for combination with angiogenesis inhibitors (32). In this study, we show that combination of agonistic CD40 antibodies with dual VEGFA/Ang2 blockade enhances antitumor responses in mouse cancer models through synergistic gene regulation and the induction of an immune permissive tumor microenvironment characterized by proinflammatory (M1-like) macrophage activation, vascular normalization, and improved infiltration and spatial localization of effector T cells.

## Results

**Combination of Anti-VEGFA, Anti-Ang2, and Agonistic Anti-CD40 Antibodies Enables Tumor Rejection in Syngeneic Tumor Models.** We examined tumor responses to anti-VEGFA, anti-Ang2, and agonistic anti-CD40 antibodies in various mouse cancer models (for details on cancer models, refer to *Materials and Methods* and *Dataset S1*). We utilized the following antibodies as antiangiogenic agents: murinized anti-Ang2 (clone LC06) (22), murinized anti-VEGFA (clone B20.4.1) (33), and a combination of anti-Ang2 and anti-VEGFA or a murinized bispecific antibody targeting the 2 proangiogenic factors (A2V) (19, 22, 24). In order to activate CD40, we used 2 anti-CD40 antibodies, clone 1C10 (murine immunoglobulin 1 [IgG1]) and clone FGK45 (rat IgG2a), which are both dependent on Fc receptor cross-linking and recognize the same CD40 epitope (34). Control mice received irrelevant IgGs or histidine buffer. Treatments and dosage regimens are described in detail in *Dataset S1*.

Single-agent treatments had modest antitumor activity compared to control IgGs in the MC38 colorectal adenocarcinoma model (Fig. 1A). Combination of Ang2 and VEGFA inhibition had additive antitumoral effects, consistent with previous studies (22). Whereas anti-CD40 only had modest inhibitory effects in combination with anti-VEGFA (1/17 tumor-free mice), it induced stabilization of tumors in a larger proportion of the mice when combined with either anti-Ang2 (6/17 tumor-free mice) or anti-VEGFA/Ang2 (9/17 tumor-free mice); notably, the combination of the 3 antibodies provided the most pronounced survival benefits (Fig. 1B). When we analyzed MC38 tumors on-therapy

in an independent experiment, we found greater intratumoral necrosis after anti-Ang2/CD40 or anti-VEGFA/Ang2/CD40 treatment, emphasizing the critical contribution of Ang2 blockade to the therapeutic response (Fig. 1C and D). Of note is that anti-CD40 monotherapy or its combination with VEGFA/Ang2 did not cause liver damage, cell dropout, or fibrosis, although a mild mononuclear infiltrate, strictly confined to portal tracts, was observed in both treatment groups (*SI Appendix, Fig. S1A*).

Analysis of other tumor models revealed additive antitumoral effects of anti-VEGFA/Ang2 plus anti-CD40. Even in established orthotopic MMTV-PyMT (mouse mammary tumor virus-polyoma virus middle-T antigen) mammary tumors, which are insensitive to anti-CD40 treatment, combined CD40 activation and VEGFA/Ang2 blockade had superior antitumoral activity, resulting in tumor growth stabilization in 3 out of 10 mice (*SI Appendix, Fig. S1B and C*). We obtained similar results in the CT26 colon carcinoma and E0771 mammary tumor models (*SI Appendix, Fig. S1E and F*). The combined treatment improved tumor control also in chicken ovalbumin (OVA)-expressing B16 melanomas (B16-OVA), which are sensitive to both VEGFA/Ang2 inhibition and CD40 activation (*SI Appendix, Fig. S1D*). Together, these results indicate that combining anti-VEGFA/Ang2 with agonistic anti-CD40 antibodies produces robust survival benefits, including tumor rejection, in different mouse models of cancer.

**Dual VEGFA/Ang2 Blockade Reprograms Tumor-Associated Blood Vessels.** We examined microvessel density (Fig. 2A–D), leakiness (Fig. 2E), and perfusion (Fig. 2F) in MC38, MMTV-PyMT, and B16-OVA tumors. The relative abundance of CD31<sup>+</sup> blood vessels was reduced by both anti-VEGFA/Ang2 and anti-VEGFA/Ang2/CD40 compared to control IgGs in the 3 models tested (Fig. 2A–D). Anti-CD40 monotherapy did not alter microvessel density compared to control tumors.

Increased leakiness and reduced perfusion of immature blood vessels may impair intratumoral drug delivery and immune cell extravasation (11). We performed intravenous (i.v.) injection of fluorescein isothiocyanate (FITC)-dextran (70 kDa) or FITC-lectin to visualize leaky and nonperfused (nonfunctional) blood vessels, respectively, in MC38 tumors (Fig. 2E and F). The fraction of nonfunctional CD31<sup>+</sup> vessels was significantly reduced in the anti-VEGFA/Ang2 and anti-VEGFA/Ang2/CD40 treatment groups, suggesting normalization and/or increased maturation of the remaining blood vessels; however, we did not observe additive effects of anti-CD40. We also performed dual NG2 and CD31 immunostaining to examine pericyte coverage, which is indicative of vascular maturation (11). We found that anti-Ang2/CD40 increased pericyte coverage of tumor blood vessels. This effect was partly limited by the addition of anti-VEGFA (Fig. 2G) and could be explained by the antiangiogenic effect of VEGFA blockade, which may contribute to decreasing maturation while improving functionality of the blood vessels (22, 24). Therefore, dual VEGFA and Ang2 inhibition induces both vascular pruning and normalization of residual blood vessels in different mouse tumor models.

**Anti-VEGFA/Ang2/CD40 Treatment Promotes Myeloid Cell Skewing in Tumors.** Anti-CD40 therapies target myeloid cell populations in tumors, leading to their activation and maturation (35–37). Dual VEGFA and Ang2 blockade was shown to promote myeloid cell activation in tumors, including M1-like tumor-associated macrophage (TAM) skewing and improved antigen presentation by DCs (22, 24). We then asked whether anti-CD40 plus VEGFA/Ang2 could cooperatively foster immunostimulatory myeloid cell activation in tumors. We observed that anti-CD40 either alone or in combination with anti-VEGFA/Ang2 markedly reduced the frequency of CD11b<sup>+</sup>Ly6C<sup>−</sup>Ly6G<sup>−</sup>F480<sup>+</sup> macrophages (TAMs) in the leukocyte infiltrate of MC38 tumors (Fig. 3A). However, the triple combination significantly decreased the proportion of CD206<sup>hi</sup>CD11c<sup>low</sup> M2-like TAMs and consequently increased the M1/M2

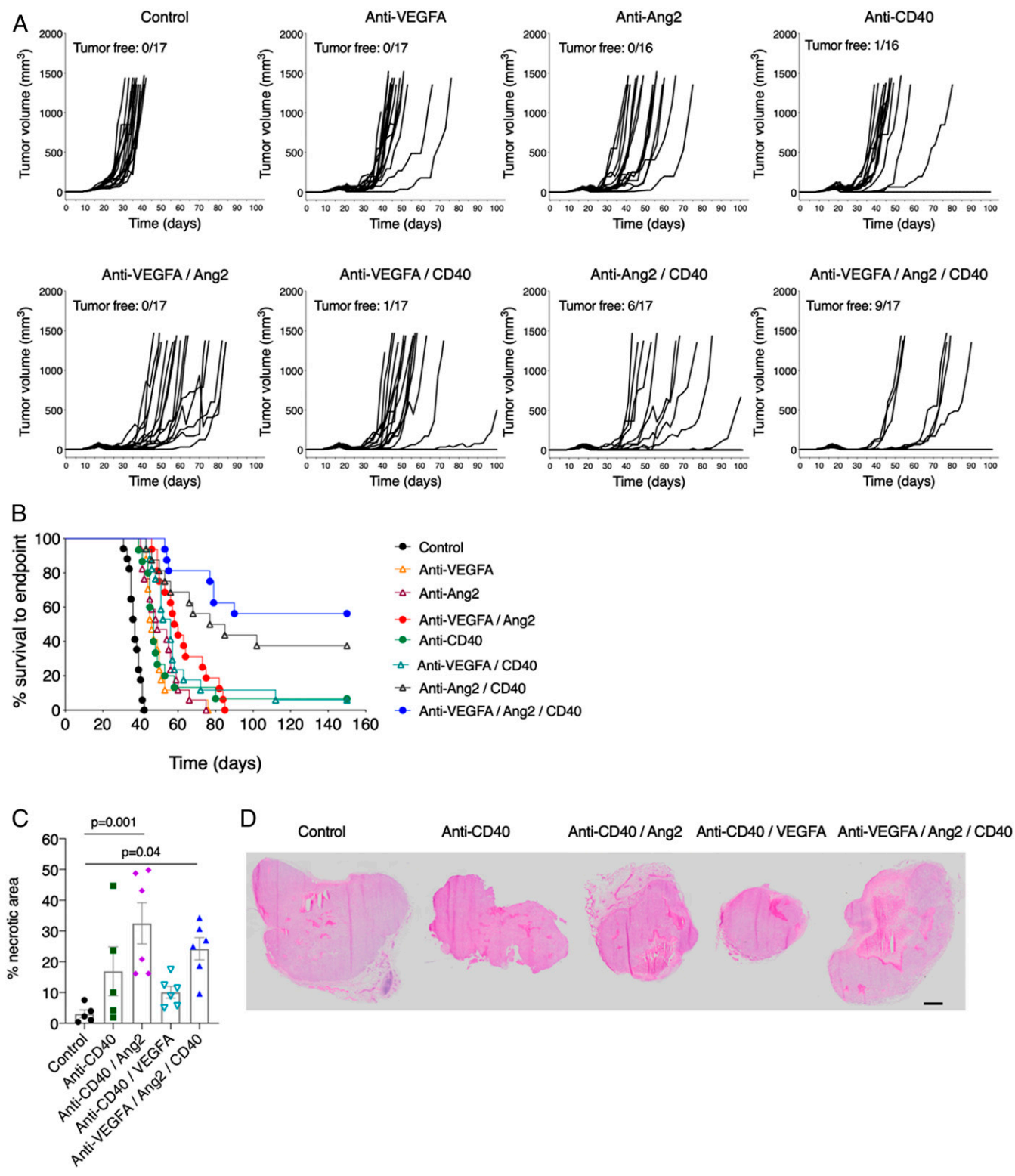


**Fig. 1.** Therapeutic efficacy of Ang2/VEGFA blockade in combination with agonistic CD40 antibodies. (A) Tumor volume and (B) Kaplan–Meier survival plot of MC38 tumors inoculated s.c. in C57BL/6 mice. Mice were treated as indicated. Anti-CD40 (1C10) or control mulgG (both at 5 mg/kg) were administered i.p. on days 18, 20, 23, and 25, whereas anti-VEGFA and anti-Ang2 (both at 10 mg/kg) were administered i.p. on days 18 and 23 postcell inoculation. Pooled data of 3 independent experiments are shown. The number of tumor-free mice out of the total number of mice, assessed at day 100 posttumor challenge, is indicated in each graph in A. (C) Relative necrotic area in MC38 tumors treated as indicated, measured in the largest tumor section. Each dot indicates one tumor. Data indicate mean values  $\pm$  SEM. Statistical analyses by 1-way ANOVA with Tukey’s correction for multiple comparisons. (D) Representative images of tumor sections stained with hematoxylin/eosin. (Scale bar, 1,000  $\mu$ m.) The number of mice employed in each experiment is reported in [Dataset S2](#).

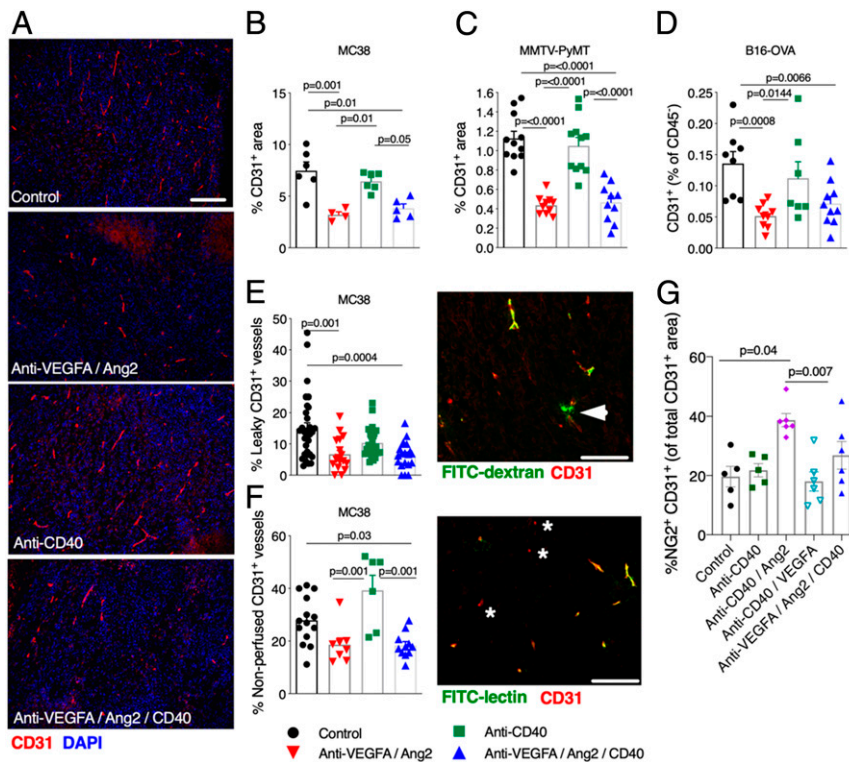


**Fig. 2.** Antiangiogenic and vascular-modulatory effects of Ang2/VEGFA blockade in combination with agonist CD40 antibodies. (A) Representative images of CD31 immunostaining (red) and DAPI nuclear staining (blue) of MC38 tumors treated with the indicated antibodies. (Scale bar, 100  $\mu\text{m}$ .) (B–D) Relative CD31<sup>+</sup> area in (B) MC38 and (C) MMTV-PyMT and (D) flow cytometry analysis of CD31<sup>+</sup> cells in B16-OVA tumors. Each data point indicates one tumor per mouse and represents an average of at least 4 images per tumor (B and C). (E) Analysis (Left) and representative image (Right) of CD31<sup>+</sup> vessels in MC38 tumors treated as indicated. Vascular leakage was identified by FITC-dextran in the abluminal compartment of CD31<sup>+</sup> blood vessels (arrowhead). Each data point represents one image; at least 3 representative images were analyzed per tumor. (Scale bar, 100  $\mu\text{m}$ .) (F) Analysis (Left) and representative image (Right) of CD31<sup>+</sup> vessels in MC38 tumors treated as indicated. Nonperfused CD31<sup>+</sup> vessels were identified by absence of FITC-lectin staining (asterisks). Each data point represents one image; at least 3 representative images were analyzed per tumor. (Scale bar, 100  $\mu\text{m}$ .) (G) Relative proportion of NG2<sup>+</sup> pericyte-covered blood vessels in MC38 tumors treated as indicated. Each dot indicates one tumor. Data indicate mean values  $\pm$  SEM. Statistical analyses by 1-way ANOVA with Tukey's correction for multiple comparisons, unless otherwise indicated in Dataset S2. The number of mice employed in each experiment is reported in Dataset S2.

TAM ratio (M1-like TAMs: CD206<sup>low</sup>CD11c<sup>hi</sup>), compared to the other treatments. In the B16-OVA model, only the combined anti-VEGFA/Ang2/CD40 treatment decreased TAMs (Fig. 3B). However, both anti-CD40 and VEGFA/Ang2 blockade decreased M2-like TAMs, and the magnitude of the effect was greater after the combined treatment. We observed similar effects on TAMs in the MMTV-PyMT model, in which only the combined treatment detectably decreased TAMs (Fig. 3C).

Intratumoral APCs, identified as CD11b<sup>+</sup>Ly6G<sup>−</sup>Ly6C<sup>−</sup>F4/80<sup>−</sup>CD11c<sup>hi</sup> cells, displayed enhanced expression of the activation and maturation markers CD86 and MHC-II after anti-VEGFA/Ang2/CD40 therapy in the B16-OVA model (Fig. 3D, Left and Middle). In the MC38-OVA model, higher MHC-II expression was observed on DCs of tumor-draining lymph node (TDLN) of mice treated with combination therapy (SI Appendix, Fig. S2A). Accordingly, the density of SIINFEKL/H-2Kb MHC-I complexes on B16-OVA tumor infiltrating APCs was higher in the anti-VEGFA/Ang2/CD40 treatment group (Fig. 3D, Right) and on APCs of TDLN of MC38-OVA tumor-bearing mice (SI Appendix, Fig. S2B), suggesting improved processing of the surrogate tumor antigen OVA by APCs through the antigen cross-presentation pathway. In agreement with previous studies (22, 24, 38), both CD40 activation and VEGFA/Ang2 blockade had stimulatory effects on APCs, although the magnitude of the effect in monotherapy was inferior to that in the combination group. Overall, these results indicate marked stimulatory activation of the innate immune cell com-

partment of tumors by combined targeting of CD40 and VEGFA/Ang2.

#### Combination of Anti-VEGFA/Ang2 and Anti-CD40 Synergistically Induces Transcriptional Changes in Macrophages, T Cells, and Endothelial Cells.

In order to identify molecular pathways and cell types directly regulated by antiangiogenic immunotherapy, we performed RNA sequencing (RNA-seq) analysis of distinct immune cell types (F4/80<sup>+</sup> TAMs, CD4<sup>+</sup>, and CD8<sup>+</sup> T cells) and CD31<sup>+</sup> endothelial cells (ECs) isolated from MMTV-PyMT tumors 5 d after treatment, as described previously (22). In clear contrast to the monotherapies, several unique genes were differentially regulated in the anti-VEGFA/Ang2/CD40 combination group, especially in CD8<sup>+</sup> T cells, macrophages, and CD31<sup>+</sup> cells (Fig. 4A and B and Datasets S3 and S4). When assessed across all treatment groups and cell types, the differential regulation was found to be cell type-specific and unique to the combination group (SI Appendix, Fig. S3A). These unique transcriptomic changes highlight the synergistic activity of anti-CD40 and anti-VEGFA/Ang2 treatment combination.

Pathway analysis in sorted TAMs revealed that anti-VEGFA/Ang2/CD40, compared to anti-CD40 monotherapy, enhanced pathways in the biofunctional groups of chemoattraction and recruitment of phagocytes/leukocytes, and activation of lymphocytes (Fig. 4C). Among the genes activated by the combined treatment in TAMs were *Cd80*, *Il12b*, and *Ccl19* (SI Appendix, Fig. S3B and C). The upstream regulators of proinflammatory pathways, namely *Tlr4*, *Trif*, *Ifng*, and *Il1b*, were overrepresented in both TAMs and ECs after combined anti-VEGFA/Ang2/CD40 treatment (Fig. 4D).

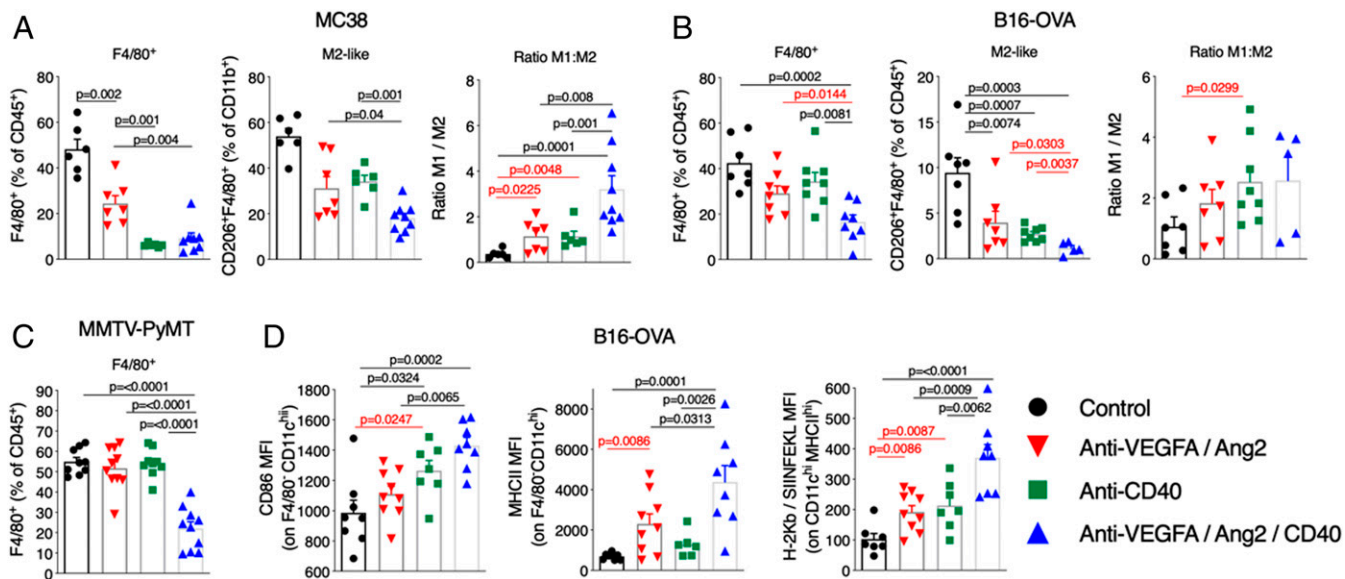


**Fig. 3.** Myeloid cell skewing by Ang2/VEGFA blockade in combination with agonist CD40 antibodies. (A) Flow cytometry analysis of tumor-infiltrating F4/80<sup>+</sup> TAMs (CD11b<sup>+</sup>Ly6G<sup>−</sup>Ly6C<sup>−</sup>F4/80<sup>+</sup>) in mice bearing MC38 tumors (Left). TAMs were further assessed for expression of the M2 marker CD206/MRC1 (Middle) and the ratio between M1 (CD11c<sup>+</sup>) and M2 (CD206<sup>+</sup>) TAMs (Right). Each data point represents one mouse. (B) Flow cytometry analyses of tumor-infiltrating TAMs (Left) as well as assessment of M2 marker (Middle) and the ratio between M1 and M2 TAMs (Right) was performed as per A in B16-OVA tumor-bearing mice. Each data point represents one mouse. (C) Flow cytometry analyses of tumor-infiltrating TAMs in mice bearing MMTV-PyMT tumors. Each data point represents one mouse. (D) Flow cytometry analysis of APCs in B16-OVA tumor-bearing mice. Data represent mean fluorescence intensity (MFI) of CD86 (Left) or MHC-II (Middle) on CD11c<sup>hi</sup> (F4/80<sup>−</sup>) APCs and MFI of SIINFEK peptide in complex with H-2Kb major histocompatibility on CD11c<sup>hi</sup>MHC-II<sup>hi</sup> APCs (Right) after gating on CD11b<sup>+</sup>Ly6G<sup>−</sup>Ly6C<sup>−</sup>F4/80<sup>−</sup> cells. Each data point represents one mouse. Data indicate mean values  $\pm$  SEM. Statistical analyses by 1-way ANOVA with Tukey's correction for multiple comparisons (black) or pairwise Student's *t* test (red), unless otherwise indicated in Dataset S2. The number of mice employed in each experiment is reported in Dataset S2.

Anti-CD40 appeared to regulate those genes in TAMs, whereas their modulation in ECs was regulated by anti-VEGFA/Ang2, as reported previously (22) (Fig. 4D). Nevertheless, the combined treatment led to enhanced activation of the aforementioned proinflammatory regulators, as well as down-regulation of suppressor of cytokine signaling 1 (*Socs1*), a negative regulator of inflammation (39) in both TAMs and ECs (Fig. 4D).

We further investigated the expression of the proinflammatory, T cell-recruiting and activating cytokines *Il12*, *Il1b*, *Cxcl9*, and *Cxcl10* in bulk MMTV-PyMT tumors by qPCR (Fig. 4E). Each gene displayed the highest induction after anti-VEGFA/Ang2/CD40 treatment, whereas anti-CD40 monotherapy and dual VEGFA/Ang2 blockade had modest, if any, effects. Collectively, these data indicate that anti-CD40–based antiangiogenic immunotherapy promotes the generation of a proinflammatory and immune-stimulatory tumor microenvironment, which may underlie the synergistic antitumoral effects observed across different tumor types.

**Anti-VEGFA/Ang2/CD40 Improves CD8<sup>+</sup> T Cell Infiltration and Promotes Their Spatial Redistribution in Tumors.** Anti-CD40 distinctly increased CD8<sup>+</sup> T cell infiltration in both MC38 and B16-OVA tumor models with little, if any, additive effects after combination with anti-VEGFA/Ang2 blocking antibodies (Fig. 5A and B). Total CD45<sup>+</sup> hematopoietic cell infiltration remained unchanged across treatment and control tumors (SI Appendix, Fig. S4A). Total CD4<sup>+</sup> T cells remained relatively unchanged in MC38 tumors and increased in both anti-CD40 and anti-VEGFA/Ang2/CD40–treated B16-OVA tumors (SI Appendix, Fig. S4B and C). However, CD4<sup>+</sup> FoxP3<sup>+</sup> regulatory T cells (Tregs) decreased in both anti-CD40 and anti-VEGFA/Ang2/CD40 treatment groups in MC38 tumors (Fig. 5C, Left), which contributed to increasing the CD8<sup>+</sup>/Treg cell ratio in the treatment groups containing anti-CD40 antibodies (Fig. 5C, Right). Accordingly, Treg gene signatures were markedly

down-regulated by anti-VEGFA/Ang2/CD40 combination in CD4<sup>+</sup> T cells isolated from MMTV-PyMT tumors (SI Appendix, Fig. S4D).

Although anti-CD40 monotherapy promoted CD8<sup>+</sup> T cell infiltration in the tumors, only its combination with anti-VEGFA/Ang2 induced tumor rejection (Fig. 1A and B). We speculated that vascular modulation by VEGFA/Ang2 blockade (Fig. 2) could improve the trafficking of tumor-reactive T cells. We, therefore, examined homing of OVA-specific CD8<sup>+</sup> T cells (OT-I cells) to MC38-OVA tumors after adoptive transfer into tumor-bearing mice. We observed increased frequency of OT-I cells in MC38-OVA tumors (Fig. 5D) but not in TDLN and spleen of mice that received the combination therapy.

We further analyzed the spatial distribution of CD8<sup>+</sup> T cells in MC38 tumors after anti-VEGFA/Ang2/CD40 treatment. We observed trends toward increased numbers of perivascular CD8<sup>+</sup> T cells in the tumors of mice that received either anti-VEGFA/Ang2 or anti-VEGFA/Ang2/CD40 antibodies, compared to the monotherapies (Fig. 5E and F). Of note is that perivascular CD8<sup>+</sup> T cells were relatively enriched in the tumor core versus periphery in the triple combination group (SI Appendix, Fig. S4E and F). When we further assessed the abundance of CD8<sup>+</sup> T cells in the periphery and core of MC38 tumors, we found that the combined treatment enhanced the infiltration of CD8<sup>+</sup> T cells to the tumor core, while CD8<sup>+</sup> T cells predominantly localized to the tumor periphery after anti-CD40 monotherapy (Fig. 5G). Consistent with these findings, we noted an enrichment in normalized blood vessels in the core of tumors, which was dependent on Ang2 blockade (SI Appendix, Fig. S4G). Together, these findings highlight the critical contribution of anti-VEGFA/Ang2–induced vascular normalization to improve trafficking of tumor-reactive CD8<sup>+</sup> T cells upon anti-CD40 immunotherapy.

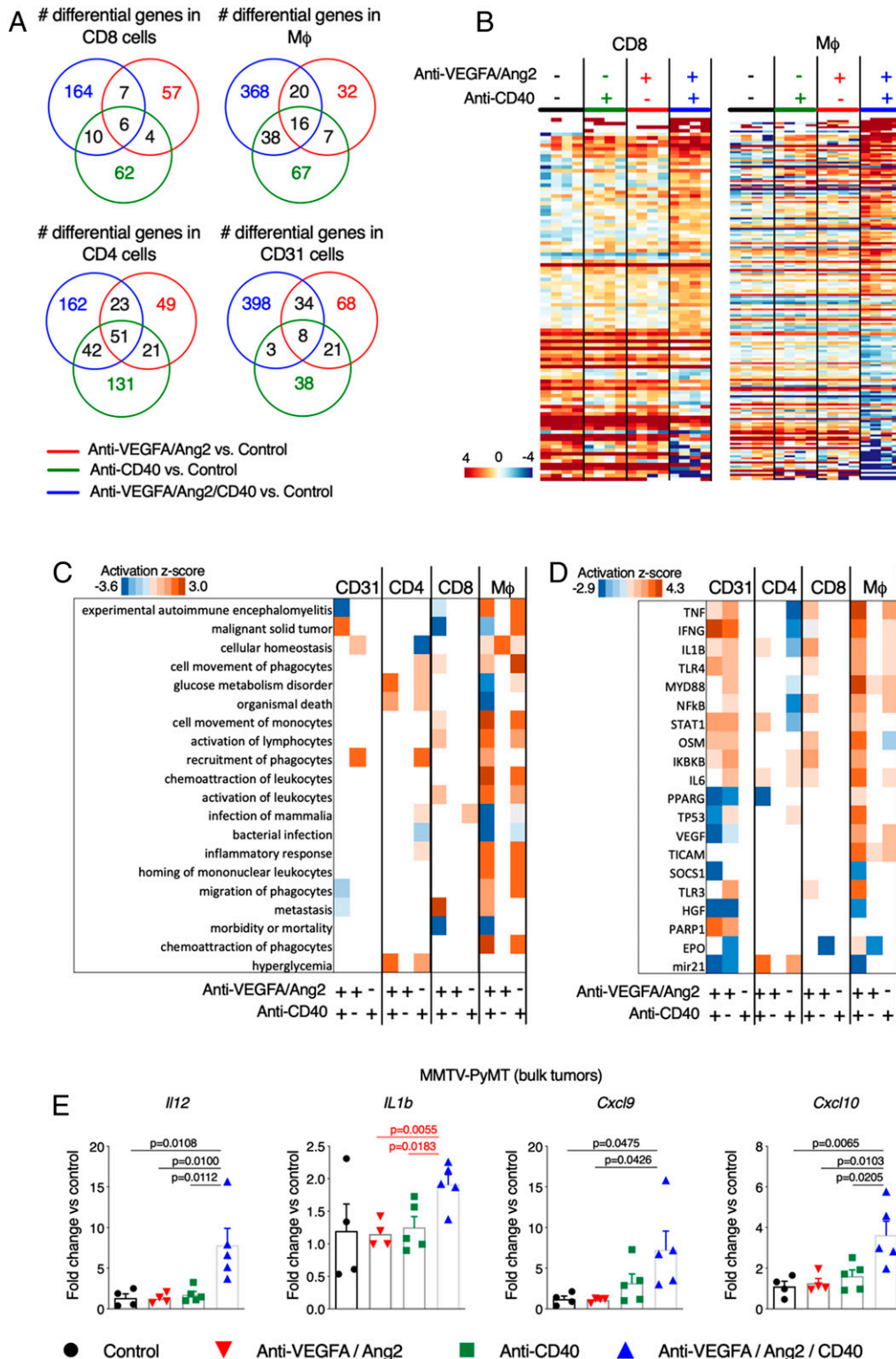


**Fig. 4.** Gene expression analysis of tumor-infiltrating immune cells and ECs. (A) Venn diagram of genes differentially expressed (up- and down-regulated compared to control IgG) according to RNA-seq in CD8<sup>+</sup>, F4/80<sup>+</sup> (M $\phi$ ), CD4<sup>+</sup>, and CD31<sup>+</sup> cells sorted from orthotopic MMTV-PyMT tumors at day 5 post-treatment (4 mice per cell type per treatment). (B) Heatmaps of genes differentially and uniquely expressed (from A) after anti-VEGFA/Ang2/CD40 treatment in CD8<sup>+</sup> cells (Left, 164 genes) and macrophages (Right, 368 genes). Expression of these genes is shown across the 4 treatment groups. (C and D) Pathway analysis scores for gene transcripts in CD31<sup>+</sup>, CD4<sup>+</sup>, CD8<sup>+</sup>, and F4/80<sup>+</sup> cells, according to bulk RNA sequencing. (E) The qPCR analysis of *Il12*, *Il1b*, *Cxcl9*, and *Cxcl10* from whole-tumor lysates of MMTV-PyMT mice at day 5 posttreatment. Data indicate the mean fold change over control (IgG treatment) after normalization to the average of *Hprt* and *Gapdh* housekeeping genes. Each data point represents one mouse. Data indicate mean values  $\pm$  SEM. Statistical analyses by 1-way ANOVA with Tukey's correction for multiple comparisons (black) or pairwise Student's *t* test (red) unless otherwise indicated in Dataset S2. The number of mice employed in each experiment is reported in Dataset S2.

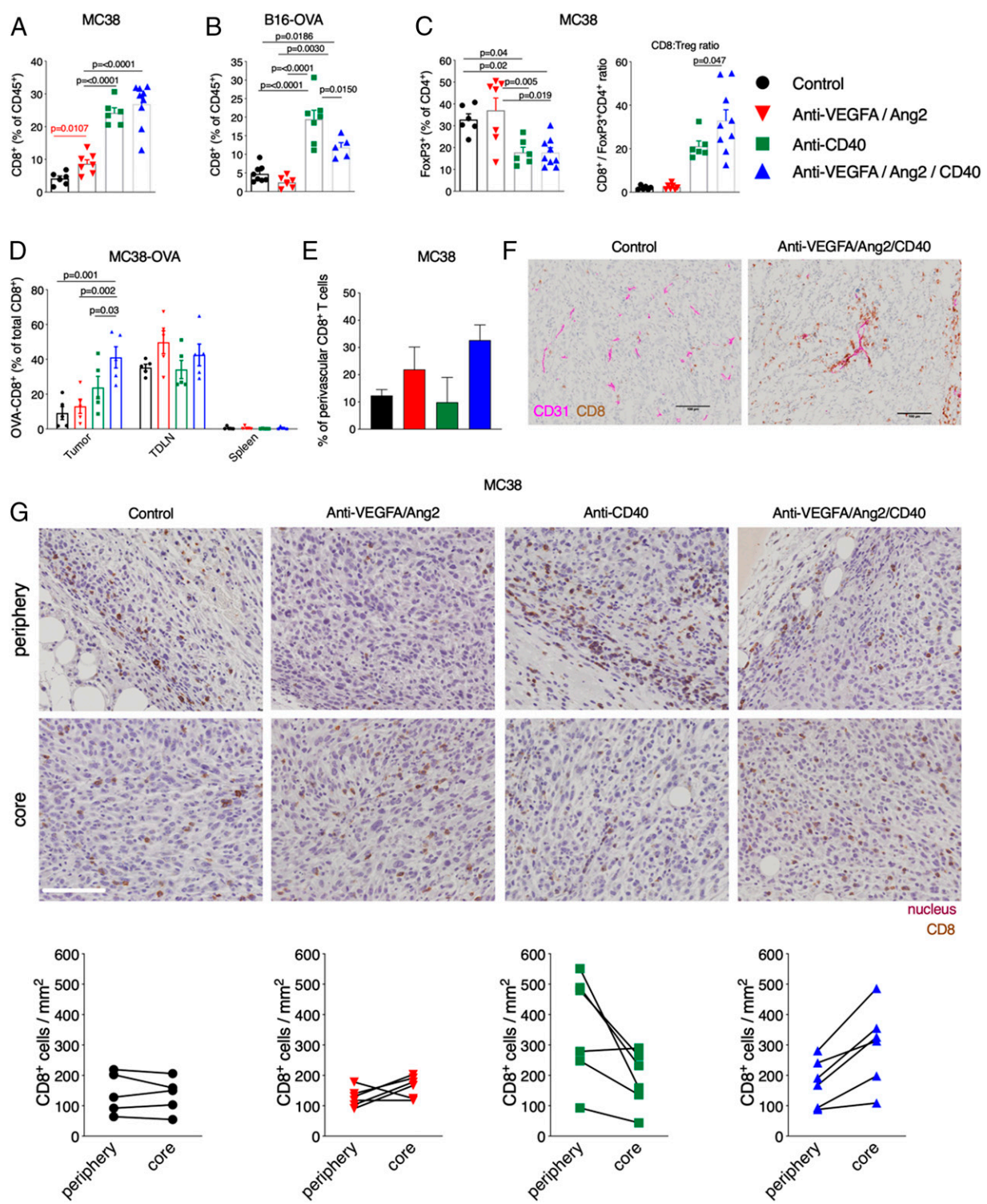


**Fig. 5.** Intratumoral T cell infiltration and spatial redistribution after Ang2/VEGFA blockade in combination with agonist CD40 antibodies. (A–C) Flow cytometry analysis of tumor-infiltrating CD8<sup>+</sup> T cells in (A) MC38 and (B) B16-OVA tumors, and (C) FoxP3<sup>+</sup> Treg cells (Left) and CD8<sup>+</sup>/Treg ratio (Right) in MC38 tumors after treatment with the indicated antibodies. Each data point represents one mouse. (D) Flow cytometry analysis of adoptively transferred OVA-specific CD8<sup>+</sup> T cells (CD8<sup>+</sup>CD45.2<sup>+</sup>CD45.1<sup>-</sup>) in tumors, TDLNs, and spleen of CD45.1<sup>+</sup>C57BL/6 mice treated as indicated. Each data point represents one mouse. (E and F) Quantification of perivascular CD8<sup>+</sup> T cells in MC38 tumors. (E) Data indicate the percentage of CD8<sup>+</sup> T cells located in the perivascular space (5 to 25  $\mu$ m from the closest CD31<sup>+</sup> blood vessel) in 2 to 3 tumors per treatment. (F) Representative images show anti-CD31 (magenta) and anti-CD8 (brown) immunostaining, and hematoxylin staining (light blue) of tumor sections. (Scale bar, 100  $\mu$ m.) (G) Intratumoral distribution of CD8<sup>+</sup> T cells in MC38 tumors. Representative images (Upper) from tumor periphery and tumor core are shown after anti-CD8 (brown) immunostaining and hematoxylin staining (light blue) of tumor sections. (Scale bar, 50  $\mu$ m.) For each tumor, the number of CD8<sup>+</sup> T cells in the tumor periphery and tumor core (>200  $\mu$ m from tumor margin) were quantified (Bottom). For each tumor, at least 4 images from each compartment were analyzed and the counts averaged. Each data point represents one mouse. Data indicate mean values  $\pm$  SEM. Statistical analyses by 1-way ANOVA with Tukey's correction for multiple comparisons (black) or pairwise Student's *t* test (red) unless otherwise indicated in Dataset S2. The number of mice employed in each experiment is reported in Dataset S2.

**Anti-VEGFA/Ang2/CD40–Based Immunotherapy Improves the Effector Functions of Intratumoral T Cells.** We next examined the functional activity of tumor-infiltrating CD8<sup>+</sup> T cells. Gene set enrichment analysis (GSEA) of RNA-seq data indicated that the combination therapy induced the highest cell cycle activity in MMTV-PyMT tumor-derived CD8<sup>+</sup> T cells, compared to other treatments (Fig. 6A). Similarly, we observed significantly higher proliferation of tumor-specific CD8<sup>+</sup> T cells (by anti-Ki67 staining) in MC38-OVA tumors, but not TDLNs, of anti-VEGFA/Ang2/CD40–treated mice (Fig. 6B, *Left*). These data suggest that anti-VEGFA/Ang2/CD40 therapy promoted the selective expansion of tumor-specific T cells in the tumor microenvironment.

We then analyzed perforin expression as a marker of T cell activation. We scored higher numbers of perforin<sup>+</sup> cells in MC38 tumors after anti-VEGFA/Ang2/CD40 therapy (Fig. 6C and D). Furthermore, the combined therapy up-regulated perforin mRNA in CD8<sup>+</sup> T cells isolated from MMTV-PyMT tumors, compared to the other treatments (Fig. 6E). In addition, the combined therapy down-regulated the Th2 signatures of CD4<sup>+</sup> T cells in these tumors (*SI Appendix, Fig. S5*), which suggested preferential skewing of the CD4<sup>+</sup> T cells toward Th1 orientation.

Taken together, these data strongly suggest that combined anti-VEGFA/Ang2/CD40 therapy promoted an antitumoral T cell phenotype that was conducive to tumor rejection in mice.

## Discussion

Although initial phase I studies of agonistic anti-CD40 monotherapy have demonstrated objective tumor responses in solid tumors (38), full therapeutic potential of CD40 agonism is likely to be realized in combination with other, nonredundant immune modulators. Herein we show that, by synergistic mechanisms with antibodies cotargeting VEGFA and Ang2, the therapeutic efficacy of agonistic CD40 antibodies in different mouse cancer types is dramatically improved. Our approach may be particularly relevant for tumors with deficient or insufficient T cell priming, a root cause of immune exclusion (2, 40). CD40 activation is a therapeutically tractable approach, which effectively stimulates antitumor immune responses proximal to T cell priming (3). Clinically relevant factors that establish a T cell-poor tumor and those that can be antagonized by anti-CD40 treatments include impaired T cell trafficking into the tumor, as well as hostile factors in the

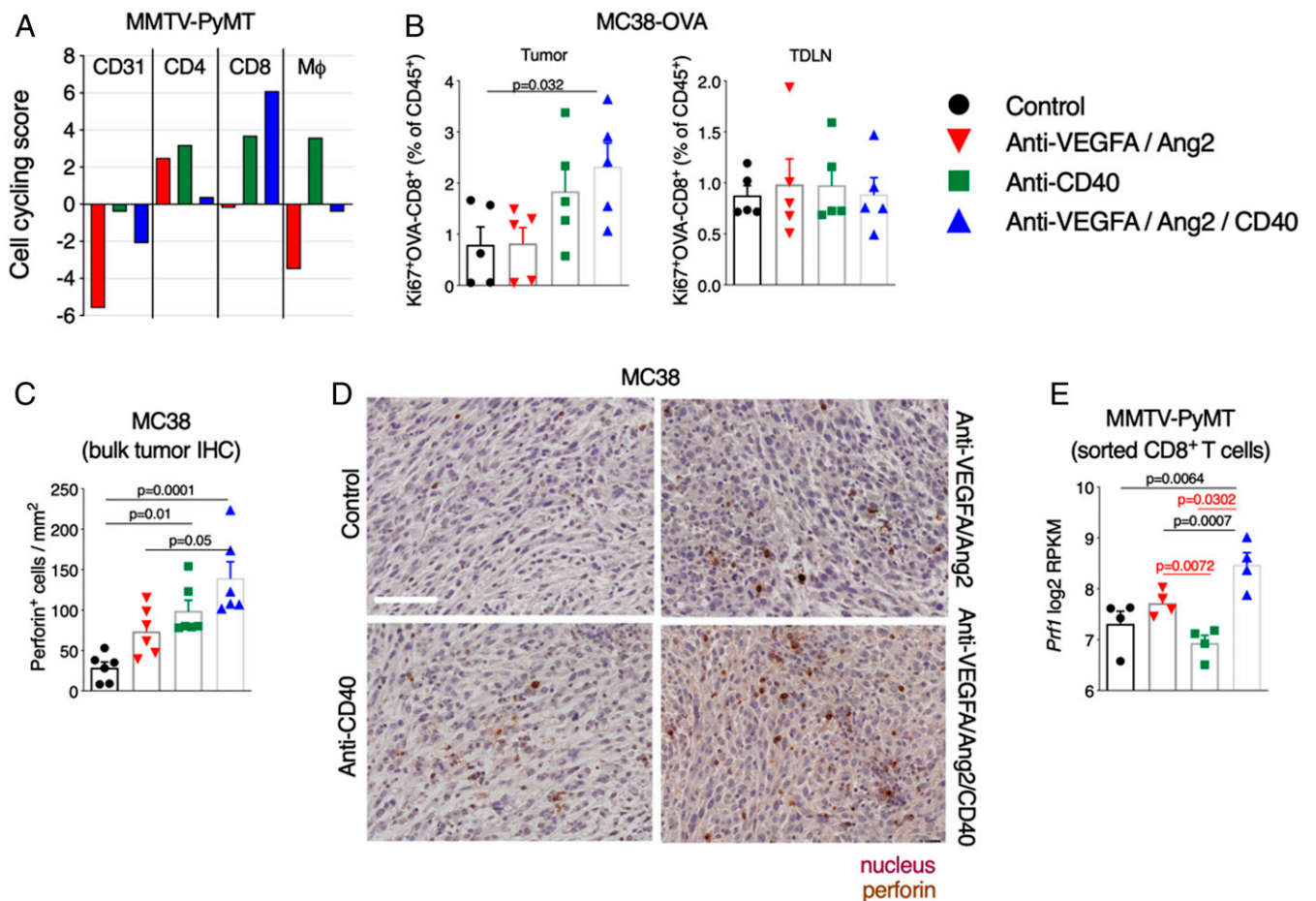


**Fig. 6.** Functional characterization of intratumoral CD8<sup>+</sup> T cells. (A) GSEA of RNA-seq data for cell cycling-related gene transcripts in cells sorted from orthotopic MMTV-PyMT tumors at day 5 posttreatment (4 mice per cell type per treatment). Positive and negative scores indicate increased and decreased cell cycling activity, respectively. (B) Flow cytometry analysis of Ki67 of adoptively transferred CD45.2<sup>+</sup> OVA-CD8<sup>+</sup> T cells in MC38-OVA tumors (*Left*) and TDLN (*Right*). Each data point represents one mouse. (C and D) Quantification of perforin<sup>+</sup> cells in MC38 tumors. (C) Data indicate the number of perforin<sup>+</sup> cells per unit of area. Each data point represents one tumor, of which at least 6 images were analyzed. (D) Representative images show antiperforin (brown) immunostaining and hematoxylin/eosin staining (light blue) of tumor sections. (Scale bar, 50  $\mu$ m.) (E) RNA sequencing of *Prf1* gene expression in CD8<sup>+</sup> T cells sorted from orthotopic MMTV-PyMT tumors at day 5 posttreatment (4 mice per treatment). Data are shown as log<sub>2</sub>-transformed RPKM (reads per kilobase per million mapped reads). Each data point represents one mouse. Data indicate mean values  $\pm$  SEM. Statistical analyses by 1-way ANOVA with Tukey's correction for multiple comparisons (black) or pairwise Student's *t* test (red) unless otherwise indicated in [Dataset S2](#). The number of mice employed in each experiment is reported in [Dataset S2](#).



tumor microenvironment that limit intratumoral T cell persistence (40). Importantly, additional key factors that control immune exclusion in the tumor are dysfunctional blood vessels mediated through aberrant angiogenesis (7). We therefore hypothesized that CD40 activation in combination with antiangiogenic VEGFA/Ang2 blockade could ultimately trigger T cell immunity and represent a clinically relevant opportunity for cancers lacking effector immune populations.

Mechanistically, we observed improved perfusion and reduced leakiness of the remaining tumor vasculature in anti-VEGFA/Ang2-treated tumors, a phenotype that was associated with increased perivascular accumulation and intratumoral infiltration of CD8<sup>+</sup> T cells. Notably, these effects on the spatial redistribution of effector T cells were independent of CD40 engagement, but essentially driven by Ang2 blockade. Stabilization or maturation of tumor microvessels was shown previously to facilitate T cell extravasation (10, 11, 22, 26, 27) and to alleviate tumor hypoxia, which improves lymphocyte function (10, 11). Various antiangiogenic agents, including bevacizumab (an anti-human VEGFA antibody), sunitinib, and axitinib (2 tyrosine kinase inhibitors that potently block tumor angiogenesis), increased tumor infiltration by both CD4<sup>+</sup> and CD8<sup>+</sup> T cells (41, 42). When combined with an agonistic anti-CD137 antibody, which activates T cells, axitinib facilitated tumor regression (42). In our study, we observed a substantial increase in the CD8<sup>+</sup>/Treg cell ratio and ablated immunosuppressive Th2 CD4<sup>+</sup> T cell signatures in tumors exposed to combinations of anti-CD40 and anti-VEGFA/Ang2 antibodies. Although anti-CD40 monotherapy increased CD8<sup>+</sup> T cell numbers per se, in line with previous studies (31, 43), only its combination with antiangiogenic antibodies promoted homing of tumor antigen-specific T cells and intratumoral infiltration of CD8<sup>+</sup> T cells. This may be a consequence of vascular normalization, chemokine secretion from the tumor microenvironment, and enhanced T cell migration to the otherwise refractory tumor microenvironment (10, 11). Improved T cell extravasation was observed previously also in human melanoma after combined bevacizumab and ipilimumab, an anti-CTLA4 antibody (44).

VEGFA/Ang2 blockade also triggered the polarization of TAMs to proinflammatory M1-like TAMs (45–47). The dual targeting of VEGFA and Ang2 was shown previously to increase M2 to M1-like skewing, which is indicative of a proinflammatory macrophage activation (22, 24, 25). In other studies, durable antitumor responses observed upon combining CD40 agonism with anti-CSF1R antibodies (36) or small-molecule CSF1R inhibitors (37, 48) were attributed to the reduction of immunosuppressive M2-like TAMs and the simultaneous induction of polyfunctional inflammatory M1-like TAMs producing TNF $\alpha$ , IL-6, and IL-12. In our study, we observed a more pronounced effect on TAM depletion after anti-CD40 therapy in MC38 tumors compared to others (36). Increased frequency of dosing and earlier time of assessment may explain such differences. Our transcriptome analysis of TAMs supports the notion that antibody-mediated CD40 activation, particularly when combined with dual VEGFA/Ang2 blockade, generates a proinflammatory tumor microenvironment characterized by enhanced production of inflammatory cytokines (IL-1 $\beta$ , IL12, IL6, and IFN $\gamma$ ) and T cell-recruiting chemokines (CXCL9 and CXCL10). This may be a consequence of the enhanced M1-like polarization of TAMs observed after combination therapy. Furthermore, the induction of NF $\kappa$ B activity and its upstream regulators TLR4 and MyD88 in TAMs may contribute to the increase of TNF $\alpha$  and other proinflammatory cytokines (49). TAM depletion would be required to assess whether in situ activated TAMs are a key effector cell population in our studies.

The addition of CD40 to dual VEGFA/Ang2 blockade further induced the maturation and/or activation of DCs. In mouse tumor models, response to agonistic CD40 therapy was shown to

be dependent on the presence of CD40-activated APCs (35), which correlated with improved activation of endogenous tumor-specific T cells (5). Blocking VEGFA and Ang2 enhances the antigen-presenting capacity of DCs in mouse tumor models (22, 50), while CD40 activation boosts adaptive immune responses through T cell priming (3). In B16-OVA tumors, the combined therapy promoted DCs to exhibit an activated phenotype characterized by enhanced expression of MHC-II and CD86 and cross-presentation of the surrogate OVA tumor antigen. Overall, T cell priming by APC activation, M1-like TAM polarization, and proinflammatory cytokine increase, in addition to vascular normalization, can contribute to sustaining the infiltration and function of tumor-reactive T cells.

The combination of agonistic CD40 antibodies and VEGFA/Ang2 blockade not only improved tumor infiltration by CD8<sup>+</sup> T cells but also enhanced their effector phenotype, namely, by increasing the proportion of proliferating, perforin-positive cells. Perforin expression may be enhanced by increased IL-12 produced in the tumor microenvironment. Indeed, both IL-12 and IL-2 directly induce perforin expression in T and NK cells, and target cell killing by CD8<sup>+</sup> T cells occurs predominantly through a perforin/granzyme-dependent degranulation mechanism (51, 52).

In summary, we report that CD40 activation in combination with dual VEGFA/Ang2 blockade improves CD8<sup>+</sup> T cell infiltration and enables tumor eradication by instigating nonredundant but synergistic immune and vascular-modulatory mechanisms. This evidence is supported by our finding that combined anti-VEGFA/Ang2/CD40 induces a unique and cell type-specific transcriptomic profile, compared to monotherapies. Our results are in line with previous studies (22, 24, 31, 36, 53), which indicated that anti-VEGFA/Ang2 and anti-CD40 monotherapies had limited therapeutic activity. Conversely, we observed tumor rejection by combining agonistic CD40 antibodies with Ang2 blockade, a result that was further improved by concomitant blockade of VEGFA. A strength of our study is that we obtained largely similar results in different tumor models and using distinct antibodies targeting CD40 and VEGFA/Ang2 (see [Dataset S1](#) for details). We consider our findings useful in the light of current early-phase clinical studies that investigate agonistic anti-CD40 antibodies in combination with various antiangiogenic agents.

## Materials and Methods

**Cell Lines and Culture.** Murine MC38 and MC38-OVA colon cancer cells (provided by Mark Smyth, Peter MacCallum Cancer Centre, Melbourne, Australia) were cultured in Dulbecco's modified Eagle's medium (Gibco) supplemented with 10% heat-inactivated fetal bovine serum (FBS; Gibco), sodium pyruvate (Sigma), penicillin/streptomycin (Gibco), 2 mM L-glutamine (Sigma), and minimal essential medium nonessential amino acids (Sigma). B16-OVA cells (provided by Karine Breckpot, Vrije Universiteit Brussel, Brussels, Belgium) were cultured in Iscove's modified Dulbecco's medium (IMDM; Sigma) supplemented with 10% FBS (Gibco), 2 mM L-glutamine (Amimed), and a combination of 50 units per mL penicillin and 50  $\mu$ g/mL streptomycin (Gibco). The cell lines used in this study were not found in the database of commonly misidentified cell lines that is maintained by the International Cell Line Authentication Committee and the National Center for Biotechnology Information. The cell lines have not been authenticated recently, but their growth behavior in vitro and in vivo was compatible with their identity. All cell lines regularly tested negative for *Mycoplasma* contamination.

**Mice.** FVB/n, BALB/c, and C57BL/6 mice were obtained from Charles River (France or Germany) or Janvier Labs (France) or bred in the animal facility of the University of Basel. OT-I, C57BL/6-Ly5.1, and FVB/n/MMTV-PyMT (22) mice were maintained and bred in house at University of Basel or EPFL (Switzerland). All mice were housed under specific pathogen-free conditions and in accordance with German and Swiss federal regulations.

**Mouse Tumor Models.** All experiments involving mice were performed according to protocols approved by the Swiss Cantonal veterinary offices of Basel-Stadt, Zurich, and Vaud (protocols 2577, 2577.a, 3049, and 3049.a to

M.D.P. and 2370, 2408, and 2589 to A.Z.). MC38 and B16-OVA tumors were generated by subcutaneous (s.c.) injection of  $0.5 \times 10^6$  or  $1 \times 10^6$  cells, respectively, in 6- to 14-wk-old C57BL/6 mice. E0771 tumor cells ( $2.5 \times 10^5$ ) were implanted orthotopically into the mammary fat pad of 6-wk-old female C57BL/6 mice. CT26 tumor cells ( $1 \times 10^6$ ) were implanted s.c. into the skin of 6-wk-old BALB/c mice. MMTV-PyMT primary tumor-derived cells ( $2 \times 10^6$ ) were implanted orthotopically into the mammary fat pad of 8- to 10-wk-old female FVB/n mice, as described previously (22). Tumors were grown for several weeks, according to either a survival schedule (endpoint defined by tumor volume) or a fixed time point (Dataset S1). Tumor size was measured by calipers, and the volume was calculated according to the formula ( $D \times d^2/2$ ), with  $D$  and  $d$  being the longest and shortest tumor diameter, respectively, in millimeters. The mice were scheduled for killing according to veterinary regulations when the tumors reached a maximum size of  $1,500 \text{ mm}^3$ . All surviving mice reflecting the tail of the curve remained tumor-free until completion of the experiments and killing.

**Therapeutic Trials in Mouse Tumor Models.** All antibodies were suspended in phosphate-buffered saline (PBS) and injected intraperitoneally (i.p.) after successful establishment of the tumors (at least 50 to  $120 \text{ mm}^3$ ). Briefly, C57BL/6 mice with MC38 tumors (treatment start at 80 to  $120 \text{ mm}^3$ ) received 2 doses of anti-VEGFA (B20.4.1, 10 mg/kg) and anti-Ang2 (LC06, 10 mg/kg), whereas anti-CD40 (1C10, 5 mg/kg) was administered 4 times. C57BL/6 mice with B16-OVA tumors (treatment start at 80 to  $120 \text{ mm}^3$ ) received bispecific anti-VEGFA/Ang2 antibody (A2V; 20 mg/kg) twice weekly and anti-CD40 (FGK45; 4 mg/kg) once after the first A2V injection. FVB/n mice with orthotopic MMTV-PyMT tumors (treatment start at about  $300 \text{ mm}^3$ ) were treated weekly with the bispecific anti-VEGFA/Ang2 antibody (A2V; 10 to 20 mg/kg), whereas anti-CD40 (FGK45; 4 mg/kg) was administered once or 3 times, depending on the experiment. C57BL/6 mice with orthotopic E0771 tumors (treatment start at 80 to  $120 \text{ mm}^3$ ) were treated with anti-VEGFA/Ang2 antibody (A2V; 10 mg/kg) weekly for up to 8 wk, whereas anti-CD40 (FGK45; 4 mg/kg) was administered once at treatment start. BALB/c mice with CT26 tumors (treatment start at 80 to  $120 \text{ mm}^3$ ) received anti-VEGFA/Ang2 antibody (A2V; 10 mg/kg) twice weekly for up to 8 wk, whereas anti-CD40 (FGK45; 4 mg/kg) was administered once at treatment start. Additional information is provided in Dataset S1.

**Preparation of Tumors, Spleen, and Lymph Nodes for Flow Cytometry.** Tumors were harvested from treated tumor-bearing mice on day 28 or 30 (for MC38 model) and day 10 or 12 (for B16-OVA model) posttumor cell injection or at study endpoint when tumors reached  $1,000 \text{ mm}^3$  (for MMTV-PyMT model), as indicated in Dataset S1. MC38 tumors were minced using razor blades followed by digestion with accutase (PAA), collagenase IV (Worthington), hyaluronidase (Sigma), and DNase type IV (Sigma) for 60 min at  $37^\circ\text{C}$  with constant shaking. B16-OVA and PyMT tumors were digested with collagenase IV (0.2 mg/mL; Worthington), dispase (2 mg/mL; Life Technologies), and DNase I (0.1 mg/mL; Life Technologies) in IMDM medium (without any supplements) for 30 min at  $37^\circ\text{C}$ . The cell suspensions were filtered using a cell strainer (70  $\mu\text{m}$ ). Spleen and LN-derived cells were isolated by mashing using the end of a 1-mL syringe. Cells were filtered through a 70- $\mu\text{m}$  nylon mesh. Red blood cells (RBCs) were lysed using RBC lysis buffer (eBioscience). Single-cell suspensions derived from tumor, spleen, and LN were blocked with rat anti-mouse Fc $\gamma$ II/III receptor (CD16/CD32) blocking antibodies ("Fc-Block") and stained with live/dead cell-exclusion dye (Zombie UV dye; Biolegend). The cells were then incubated with fluorophore-conjugated antibodies directed against cell surface antigens, washed, and resuspended in fluorescence-activated cell sorter (FACS) buffer (PBS + 2% FBS). For intracellular antigens (FoxP3 and Ki67), cells stained with cell surface antibodies were fixed (IC fix; eBioscience) and permeabilized (Perm buffer; eBioscience) prior to incubation with antibodies directed at intracellular antigens. Cell populations were analyzed on BD Fortessa. Flow cytometry analysis of cell populations were performed on BD Fortessa (as per SI Appendix).

**Adoptive Transfer of OT-I Cells in MC38-OVA Tumor-Bearing Mice.** OVA-specific CD8<sup>+</sup> T cells were obtained from spleen and inguinal and axial lymph nodes of OT-I TCR transgenic C57BL/6 mice (Ly5.2). The CD8<sup>+</sup> T cell negative selection kit (Stemcell Technologies) was used to isolate a pure population of CD8<sup>+</sup> T cells (98% CD8<sup>+</sup> T cells as determined by FACS). OT-I T cells were then cultured in 10-cm plates prebound with anti-CD3 and anti-CD28 antibodies (10  $\mu\text{g}/\text{mL}$  each) for 72 h in Roswell Park Memorial Institute (RPMI) medium +10% FBS. On day 22 posttumor cell injection,  $2 \times 10^6$  OT-I cells were injected i.v. into MC38-OVA-bearing C57BL/6 (Ly5.1) mice. Eight days post-OT-I adoptive transfer (day 30 posttumor cell injection), mice were killed,

and tumor and TDLNs (right inguinal and axial lymph nodes) were collected for assessment by flow cytometry (as per SI Appendix).

**In Vivo Labeling of Functional Tumor Blood Vessels for Assessment of Leakiness and Perfusion.** Blood vessel leakiness and perfusion was assessed on day-28 MC38 tumors in terminally anesthetized mice. Leaky blood vessels were detected by i.v. injecting 250  $\mu\text{g}$  of fluorescein-labeled dextran (70 kDa, D-1822; Life Technologies) in 200  $\mu\text{L}$  of PBS. After a circulation time of 5 min, the mice were first perfused via the left cardiac ventricle with PBS and subsequently with 4% paraformaldehyde (PFA). For the detection of perfused blood vessels, 100  $\mu\text{g}$  of fluorescein-labeled lycopersicon esculentum (tomato) lectin (GL-1171; Vector Laboratories) was injected in 100  $\mu\text{L}$  of PBS i.v. via the tail vein. After a circulation time of 4 min, the mice were perfused with 4% PFA followed by PBS via the left cardiac ventricle. Tumors were frozen and embedded in Tissue-Tek optimal cutting temperature compound using standard protocols, and stored at  $-80^\circ\text{C}$ . The tissues were cut into 8- $\mu\text{m}$ -thick sections using a cryotome and dried for 30 min at room temperature protected from light. Subsequently, tissue sections were rehydrated in PBS for 5 min, permeabilized in PBS/0.1% Triton X-100 for 20 min, and blocked with PBS/5% normal goat serum (ngs; Sigma). The rat anti-CD31 antibody (550274; BD Pharmingen) was diluted 1:50 in PBS/5% ngs and used for incubating the slides overnight in a humid chamber at  $4^\circ\text{C}$ . The slides were subsequently washed 3 times for 5 min in PBS and incubated with the secondary anti-rat Alexa 568 antibody (molecular probes; 1:200 in PBS/5% ngs). After a washing step of 3 times 5 min, nuclei were stained with DAPI (1:10,000 Sigma), and slides were mounted with Dako mounting medium (Dako) and stored in the dark ( $4^\circ\text{C}$ ) until analysis.

**Immunostaining.** Formalin-fixed paraffin-embedded tumors or fresh frozen tumors were prepared for immunostaining of CD8<sup>+</sup> T cells, CD31<sup>+</sup>, and/or NG2<sup>+</sup> tumor blood vessels as per SI Appendix. The immunostained tumors were then analyzed using ImageJ for assessment of tumor necrosis, percentage of pericyte-covered blood vessels, and perivascular CD8<sup>+</sup> T cells as per SI Appendix.

**Sorting of MMTV-PyMT Tumor-Derived Cells for RNA-seq.** Orthotopic MMTV-PyMT tumors were generated as described above, and cells were sorted and analyzed as described previously (22). When tumors reached a size of about  $300 \text{ mm}^3$ , mice were injected i.p. with the antibodies indicated in Dataset S1. Five days later, mice were killed, and tumors were harvested and prepared for flow cytometry staining as described above. Cells were stained for CD45, CD8, CD4, CD31, CD11b, F480, and 7-AAD. After live/dead and single-cell discrimination, cell populations were discriminated according to the following markers: ECs: CD45<sup>-</sup>CD31<sup>+</sup>; TAMs: CD45<sup>+</sup>CD11b<sup>+</sup>F480<sup>+</sup>; CD8<sup>+</sup> T cells: CD45<sup>+</sup>CD11b<sup>-</sup>CD8<sup>+</sup>; CD4<sup>+</sup> T cells: CD45<sup>+</sup>CD11b<sup>-</sup>CD4<sup>+</sup>. Cell sorting was performed using FACS Aria II (BD). Each cell population ( $n = 4$ ) was isolated from an independent tumor. Typically,  $2 \times 10^4$  to  $2 \times 10^5$  cells were obtained for each cell population.

**RNA-seq and Computational Signature Analysis.** RNA-seq of sorted cell populations was performed and analyzed as recently described by us (22, 47). The gene expression cutoffs to classify up and down-regulated genes compared to control IgG were set as follows: raw  $P$  values less than 0.05 and absolute  $\log_2$  ratio greater than 1. Data are deposited in NCBI Gene Expression Omnibus (GEO) under GSE94920. GSEA-like signature analysis on transcriptome-wide gene expression values was performed using the function signedRankSumTest from the gCMAP package (54). This analysis generated Wilcoxon/Mann-Whitney rank sum statistics representing the activation level or likelihood level of the pathway or phenotype characterized by a signature in a treatment group compared to another, with an associated  $P$  value to denote the statistical significance. Signatures were obtained from Molecular Signatures Database (55). Pathway analysis for only genes that passed criteria of raw  $P$  value less than 0.05 and absolute  $\log_2$  fold change of more than 1 was performed using Ingenuity Pathway Analysis software.

**Statistical Analysis.** Detailed statistical analyses are described in SI Appendix. Statistical significance is indicated in the figures as follows:  $*0.01 \leq P < 0.05$ ;  $**0.001 \leq P < 0.01$ ;  $***P < 0.001$ .  $P$  values  $> 0.05$  are not indicated. "N" values are indicated in Dataset S2. On rare occasions, outliers at the endpoint were excluded by using the ROUT (robust regression followed by outlier identification) method (provided in GraphPad Prism) to identify outliers. In some cases, selected samples were excluded from specific analyses because of technical flaws during sample processing or data acquisition.

**Data and Materials Availability.** Primary RNA-seq data sets have been deposited in the Gene Expression Omnibus (GEO), <https://www.ncbi.nlm.nih.gov/geo/> under accession code GSE94920. A2V, LC06, B20, and isotype-matched control IgGs were provided by Roche under conditions expressed in sponsored research agreements between Roche and the corresponding authors' institutions (University of Basel and EPFL). Interested researchers may contact Roche for requests concerning the aforementioned materials.

**ACKNOWLEDGMENTS.** We thank H. Sade (Roche Innovation Center Munich, Pathology) for support with immunohistochemistry staining; D. Laoui (Vrije Uni-

versiteit Brussel [VUB], Brussels, Belgium) for advice on experimental design; C. Wyser-Rmili, A. Bellotti, C. Piot (all from EPFL), S. Hoert, and C. Bayer (both from Roche Innovation Center Munich, Pharmacology) for experimental help; the Flow Cytometry and Bioluminescence and Optics core facilities at EPFL and University of Basel for help with cell sorting and image analysis; K. Breckpot (VUB) for providing B16-OVA cells; and N. Haynes (University of Melbourne) and Mark Smyth (Queensland Institute of Medical Research, Australia) for providing MC38 and MC38-OVA cells, respectively. M.D.P. acknowledges grant support from the Swiss Cancer League (Grant KFS-3759-08-2015), Leenaards Foundation, San Salvatore Foundation, and Roche. A.Z. acknowledges grant support from the Swiss Cancer League (Grant KFS-3394-02-2014) and Roche.

- J. A. Seidel, A. Otsuka, K. Kabashima, Anti-PD-1 and anti-CTLA-4 therapies in cancer: Mechanisms of action, efficacy, and limitations. *Front. Oncol.* **8**, 86 (2018).
- P. Sharma, S. Hu-Lieskovan, J. A. Wargo, A. Ribas, Primary, adaptive, and acquired resistance to cancer immunotherapy. *Cell* **168**, 707–723 (2017).
- R. H. Vonderheide, The immune revolution: A case for priming, not checkpoint. *Cancer Cell* **33**, 563–569 (2018).
- R. H. Vonderheide, M. J. Glennie, Agonistic CD40 antibodies and cancer therapy. *Clin. Cancer Res.* **19**, 1035–1043 (2013).
- E. M. Sotomayor *et al.*, Conversion of tumor-specific CD4+ T-cell tolerance to T-cell priming through in vivo ligation of CD40. *Nat. Med.* **5**, 780–787 (1999).
- S. B. Hassan, J. F. Sørensen, B. N. Olsen, A. E. Pedersen, Anti-CD40-mediated cancer immunotherapy: An update of recent and ongoing clinical trials. *Immunopharmacol. Immunotoxicol.* **36**, 96–104 (2014).
- M. De Palma, D. Bizziato, T. V. Petrova, Microenvironmental regulation of tumour angiogenesis. *Nat. Rev. Cancer* **17**, 457–474 (2017).
- D. P. Bottaro, L. A. Liotta, Cancer: Out of air is not out of action. *Nature* **423**, 593–595 (2003).
- M. Schmittnaegel, M. De Palma, Reprogramming tumor blood vessels for enhancing immunotherapy. *Trends Cancer* **3**, 809–812 (2017).
- G. T. Motz, G. Coukos, The parallel lives of angiogenesis and immunosuppression: Cancer and other tales. *Nat. Rev. Immunol.* **11**, 702–711 (2011).
- R. K. Jain, Antiangiogenesis strategies revisited: From starving tumors to alleviating hypoxia. *Cancer Cell* **26**, 605–622 (2014).
- N. Ferrara, A. P. Adamis, Ten years of anti-vascular endothelial growth factor therapy. *Nat. Rev. Drug Discov.* **15**, 385–403 (2016).
- A. Scholz *et al.*, Endothelial cell-derived angiopoietin-2 is a therapeutic target in treatment-naïve and bevacizumab-resistant glioblastoma. *EMBO Mol. Med.* **8**, 39–57 (2016).
- P. Saharinen, L. Eklund, K. Alitalo, Therapeutic targeting of the angiopoietin-TIE pathway. *Nat. Rev. Drug Discov.* **16**, 635–661 (2017).
- N. Rigamonti *et al.*, Role of angiopoietin-2 in adaptive tumor resistance to VEGF signaling blockade. *Cell Rep.* **8**, 696–706 (2014).
- A. S. Chung, J. Lee, N. Ferrara, Targeting the tumour vasculature: Insights from physiological angiogenesis. *Nat. Rev. Cancer* **10**, 505–514 (2010).
- R. Mazziere *et al.*, Targeting the ANG2/TIE2 axis inhibits tumor growth and metastasis by impairing angiogenesis and disabling rebounds of proangiogenic myeloid cells. *Cancer Cell* **19**, 512–526 (2011).
- C. Daly *et al.*, Angiopoietin-2 functions as a Tie2 agonist in tumor models, where it limits the effects of VEGF inhibition. *Cancer Res.* **73**, 108–118 (2013).
- Y. Kienast *et al.*, Ang-2-VEGF-A CrossMab, a novel bispecific human IgG1 antibody blocking VEGF-A and Ang-2 functions simultaneously, mediates potent antitumor, antiangiogenic, and antimetastatic efficacy. *Clin. Cancer Res.* **19**, 6730–6740 (2013).
- K. Srivastava *et al.*, Postsurgical adjuvant tumor therapy by combining anti-angiopoietin-2 and metronomic chemotherapy limits metastatic growth. *Cancer Cell* **26**, 880–895 (2014).
- H. Hashizume *et al.*, Complementary actions of inhibitors of angiopoietin-2 and VEGF on tumor angiogenesis and growth. *Cancer Res.* **70**, 2213–2223 (2010).
- M. Schmittnaegel *et al.*, Dual angiopoietin-2 and VEGFA inhibition elicits antitumor immunity that is enhanced by PD-1 checkpoint blockade. *Sci. Transl. Med.* **9**, eaak9670 (2017).
- Y. J. Koh *et al.*, Double antiangiogenic protein, DAAP, targeting VEGF-A and angiopoietins in tumor angiogenesis, metastasis, and vascular leakage. *Cancer Cell* **18**, 171–184 (2010).
- J. Klopper *et al.*, Ang-2/VEGF bispecific antibody reprograms macrophages and resident microglia to anti-tumor phenotype and prolongs glioblastoma survival. *Proc. Natl. Acad. Sci. U.S.A.* **113**, 4476–4481 (2016).
- T. E. Peterson *et al.*, Dual inhibition of Ang-2 and VEGF receptors normalizes tumor vasculature and prolongs survival in glioblastoma by altering macrophages. *Proc. Natl. Acad. Sci. U.S.A.* **113**, 4470–4475 (2016).
- D. Fukumura, J. Klopper, Z. Amoozgar, D. G. Duda, R. K. Jain, Enhancing cancer immunotherapy using antiangiogenics: Opportunities and challenges. *Nat. Rev. Clin. Oncol.* **15**, 325–340 (2018).
- E. Allen *et al.*, Combined antiangiogenic and anti-PD-L1 therapy stimulates tumor immunity through HEV formation. *Sci. Transl. Med.* **9**, eaak9679 (2017).
- P. A. Ott, F. S. Hodi, E. I. Buchbinder, Inhibition of immune checkpoints and vascular endothelial growth factor as combination therapy for metastatic melanoma: An overview of rationale, preclinical evidence, and initial clinical data. *Front. Oncol.* **5**, 202 (2015).
- M. A. Socinski *et al.*, IMpower150 Study Group, Atezolizumab for first-line treatment of metastatic nonsquamous NSCLC. *N. Engl. J. Med.* **378**, 2288–2301 (2018).
- H. D. Lum *et al.*, In vivo CD40 ligation can induce T-cell-independent antitumor effects that involve macrophages. *J. Leukoc. Biol.* **79**, 1181–1192 (2006).
- A. Zippelius, J. Schreiner, P. Herzog, P. Müller, Induced PD-L1 expression mediates acquired resistance to agonistic anti-CD40 treatment. *Cancer Immunol. Res.* **3**, 236–244 (2015).
- S. Selvaraj, M. Raundhal, A. Patidar, B. Saha, Anti-VEGF antibody enhances the antitumor effect of CD40. *Int. J. Cancer* **135**, 1983–1988 (2014).
- W.-C. Liang *et al.*, Cross-species vascular endothelial growth factor (VEGF)-blocking antibodies completely inhibit the growth of human tumor xenografts and measure the contribution of stromal VEGF. *J. Biol. Chem.* **281**, 951–961 (2006).
- L. P. Richman, R. H. Vonderheide, Role of crosslinking for agonistic CD40 monoclonal antibodies as immune therapy of cancer. *Cancer Immunol. Res.* **2**, 19–26 (2014).
- G. L. Beatty *et al.*, CD40 agonists alter tumor stroma and show efficacy against pancreatic carcinoma in mice and humans. *Science* **331**, 1612–1616 (2011).
- S. Hoves *et al.*, Rapid activation of tumor-associated macrophages boosts preexisting tumor immunity. *J. Exp. Med.* **215**, 859–876 (2018).
- C. J. Perry *et al.*, Myeloid-targeted immunotherapies act in synergy to induce inflammation and antitumor immunity. *J. Exp. Med.* **215**, 877–893 (2018).
- R. H. Vonderheide *et al.*, Clinical activity and immune modulation in cancer patients treated with CP-870,893, a novel CD40 agonist monoclonal antibody. *J. Clin. Oncol.* **25**, 876–883 (2007).
- S. Chikuma, M. Kanamori, S. Mise-Omata, A. Yoshimura, Suppressors of cytokine signaling: Potential immune checkpoint molecules for cancer immunotherapy. *Cancer Sci.* **108**, 574–580 (2017).
- S. Spranger, T. F. Gajewski, Impact of oncogenic pathways on evasion of antitumor immune responses. *Nat. Rev. Cancer* **18**, 139–147 (2018).
- X. D. Liu *et al.*, Resistance to antiangiogenic therapy is associated with an immunosuppressive tumor microenvironment in metastatic renal cell carcinoma. *Cancer Immunol. Res.* **3**, 1017–1029 (2015).
- H. Läubli *et al.*, The multi-receptor inhibitor axitinib reverses tumor-induced immunosuppression and potentiates treatment with immune-modulatory antibodies in preclinical murine models. *Cancer Immunol. Immunother.* **67**, 815–824 (2018).
- S. F. Ngwi *et al.*, Agonistic CD40 mAb-driven IL12 reverses resistance to anti-PD1 in a T-cell-rich tumor. *Cancer Res.* **76**, 6266–6277 (2016).
- F. S. Hodi *et al.*, Bevacizumab plus ipilimumab in patients with metastatic melanoma. *Cancer Immunol. Res.* **2**, 632–642 (2014).
- S. K. Biswas, A. Mantovani, Macrophage plasticity and interaction with lymphocyte subsets: Cancer as a paradigm. *Nat. Immunol.* **11**, 889–896 (2010).
- R. Noy, J. W. Pollard, Tumor-associated macrophages: From mechanisms to therapy. *Immunity* **41**, 49–61 (2014).
- C. Baer *et al.*, Suppression of microRNA activity amplifies IFN- $\gamma$ -induced macrophage activation and promotes anti-tumor immunity. *Nat. Cell Biol.* **18**, 790–802 (2016).
- R. Manyevitch *et al.*, Evaluation of metabolic and synaptic dysfunction hypotheses of Alzheimer's Disease (AD): A meta-analysis of CSF markers. *Curr. Alzheimer Res.* **15**, 164–181 (2018).
- T. Kawasaki, T. Kawai, Toll-like receptor signaling pathways. *Front. Immunol.* **5**, 461 (2014).
- D. I. Gabrilovich *et al.*, Production of vascular endothelial growth factor by human tumors inhibits the functional maturation of dendritic cells. *Nat. Med.* **2**, 1096–1103 (1996).
- T. W. Salcedo, L. Azzone, S. F. Wolf, B. Perussia, Modulation of perforin and granzyme messenger RNA expression in human natural killer cells. *J. Immunol.* **151**, 2511–2520 (1993).
- M. E. Pipkin, A. Rao, M. G. Lichtenheld, The transcriptional control of the perforin locus. *Immunol. Rev.* **235**, 55–72 (2010).
- K. R. Wiehagen *et al.*, Combination of CD40 agonism and CSF-1R blockade reconditions tumor-associated macrophages and drives potent antitumor immunity. *Cancer Immunol. Res.* **5**, 1109–1121 (2017).
- T. Sandmann, S. K. Kummerfeld, R. Gentleman, R. Bourgon, gCMAP: User-friendly connectivity mapping with R. *Bioinformatics* **30**, 127–128 (2014).
- A. Subramanian *et al.*, Gene set enrichment analysis: A knowledge-based approach for interpreting genome-wide expression profiles. *Proc. Natl. Acad. Sci. U.S.A.* **102**, 15545–15550 (2005).